

# Critical Currents and Vortex States at Fractional Matching Fields in Superconductors with Periodic Pinning

Charles Reichhardt

*Department of Physics, University of California, Davis, California 95616.*

Niels Grønbech-Jensen

*Department of Applied Science, University of California, Davis, California 95616.*

*NERSC, Lawrence Berkeley National Laboratory, Berkeley, California 94720.*

(October 26, 2018)

We study vortex states and dynamics in 2D superconductors with periodic pinning at fractional sub-matching fields using numerical simulations. For square pinning arrays we show that ordered vortex states form at  $1/1, 1/2$ , and  $1/4$  filling fractions while only partially ordered states form at other filling fractions, such as  $1/3$  and  $1/5$ , in agreement with recent imaging experiments. For triangular pinning arrays we observe matching effects at filling fractions of  $1/1, 6/7, 2/3, 1/3, 1/4, 1/6$ , and  $1/7$ . For both square and triangular pinning arrays we also find that, for certain sub-matching fillings, vortex configurations depend on pinning strength. For weak pinning, ordering in which a portion of the vortices are positioned between pinning sites can occur. Depinning of the vortices at the matching fields, where the vortices are ordered, is elastic while at the incommensurate fields the motion is plastic. At the incommensurate fields, as the applied driving force is increased, there can be a transition to elastic flow where the vortices move along the pinning sites in 1D channels and a reordering transition to a triangular or distorted triangular lattice. We also discuss the current-voltage curves and how they relate to the vortex ordering at commensurate and incommensurate fields.

## I. INTRODUCTION

Vortex lattices interacting with quenched disorder represent an ideal system in which to study various static and dynamic phases of elastic lattices in disordered media, which can be found in a large class of condensed matter systems. Pinning of vortices is also of practical importance since superconductors are required to maintain high critical currents for various potential technological applications. There have been considerable efforts to enhance the pinning properties of vortices in superconductors by introducing point, columnar, and splay defects using electron, proton and heavy ion irradiation [1]. A particularly promising technique has been to lithographically create nano-structured periodic defect arrays. Experiments with arrays of holes [2–13] and magnetic dots [14–19], as well as theory [20] and numerical simulations [21], have shown that a variety of commensurability effects occur when the density of vortices equals an integer multiple of the density of pinning sites such that a well ordered vortex crystal can be stabilized and pinned. Several experiments have provided evidence that for small pinning sites, beyond the first matching field, a portion of the vortices will sit at the interstitial regions between the pinning sites [6,10].

Besides matching effects at integer filling fractions, commensurability effects at non-integer and sub-matching fields have also been observed directly with Lorentz microscopy [10] and indirectly with magnetization and transport measurements [4–6]. Experiments by

Metlushko *et al.* observed sub-matching effects down to  $1/16$  filling fractions [5]. These same experiments did not show any particular fractional matching for  $B/B_\phi > 1.0$ . In other experiments, fractional matching has been seen at filling fractions of  $3/2$  and  $5/2$  [11]. These fractional matching effects are generally less pronounced than those of the integer matching fields.

Recent scanning-Hall probe measurements have also directly imaged vortex configurations at various sub-matching fields [12,13]. These measurements find that some configurations are only partially ordered while others, including the integer matching fields, are almost completely ordered. Experiments by Field *et al.*, who image up to 5,000 vortices, have found that at the  $1/2$  matching field very large regions of ordered vortex checkerboard states can be observed with well defined domain walls separating different orientations [12]. At other fields, such as  $1/3$ , only domains of diagonally ordered regions are observed, while at  $1/4, 2/5$ , and  $1/5$  even smaller regions of order are observed.

Previous simulations of vortices interacting with periodic pinning arrays have focused on vortex matching at integer matching fields and have found that different types of vortex crystals can be stabilized at different matching fields in agreement with experiments [21]. The case of vortex matching at fractional fields for square and triangular pinning arrays has not been addressed. Although commensurate vortex configurations in Josephson-junction arrays [22] and repulsive particles on lattices [23] at fractional fillings have been studied, these models do not allow the vortices to sit at intersti-

tial regions between the pinning sites as is possible in experiments with periodic pinning, magnetic dot, or hole arrays. For  $B/B_\phi > 1$  it is clear that interstitial pinning of vortices is possible. In this work we show that for certain pinning strengths and commensurabilities it is possible for a portion of the vortices to be positioned at interstitial sites even for  $B/B_\phi < 1$ , so that the vortices form a type of ordering that would be absent for vortices in wire networks and Josephson-junction arrays. Further, the dynamic phases are also strongly affected by the fact that vortex flow can occur through the interstitial regions.

For *random pinning* sites, theory [24–26], simulations [24,27,28] and experiments [29–31] find that an initially pinned disordered vortex lattice can first flow plastically and then undergo a dynamic transition from a disordered structure to an ordered moving vortex lattice which can be a moving Bragg glass or moving smectic phase. The vortices in the strongly driven phase flow in well defined channels and a transverse depinning threshold can be present [25]. Similarly, in simulations with *periodic pinning* where the vortex density exceeds the pinning density,  $B/B_\phi > 1$ , distinct kinds of plastic flow and large transverse barriers may exist [32]. Simulations of Josephson-junction arrays have also found plastic and elastic vortex flow phases and transverse depinning transitions [33,34].

The dynamics of vortices in periodic pinning arrays with  $B/B_\phi < 1$  has not previously been studied. For this case, some of the open questions are (i) whether the vortex configurations in the pinned state are the same as the moving vortex configuration; (ii) how this depends on the filling fraction; and (iii) whether there can be plastic flow and how it depends on commensurability. Unlike systems with random pinning, where the disorder comes from the quenched substrate, the disorder in vortex systems with periodic pinning comes about from the vortex-vortex interactions with the incommensurate fields forming a disordered vortex lattice. At the commensurate fields, where the vortex lattice is ordered, plastic flow may be absent even though the vortex lattice is very strongly pinned. At strong driving forces it may be interesting to see if the incommensurate vortex lattice can reorder to a moving crystal phase in a similar manner as observed in systems with random pinning. It may also be interesting to compare commensurate and incommensurate fields in strongly driven phases to see whether the vortex flow occurs in 1D channels and if the flow is between or along the pinning rows. It may further be valuable to correlate the microscopics of the static and dynamical phases to macroscopic observables, such as critical currents, current-voltage characteristics, and magnetization.

In this work we examine the vortex configurations and dynamics for square and triangular pinning arrays in 2D superconductors with logarithmically interacting vortices

using molecular dynamics simulations of pancake vortices. For the square pinning array we find a series of sub-matching effects that can be seen as peaks in the critical depinning force. The vortex configurations at these fields agree well with those seen in recent imaging experiments [10,12,13]. Certain sub-matching fields, such as  $1/3$  are not completely ordered, but are broken up into domains as also observed in experiments [12]. Vortex ordering at  $1/3$  filling depends on the pinning strength with stronger pinning producing a partially diagonally ordered arrangement. For weak disorder at  $1/3$  filling we observe a vortex ordering in which certain vortices sit in the interstitial regions between the pinning sites so that the overall vortex lattice has a near triangular ordering. We also find that the critical depinning force increases linearly with pinning force strength at the commensurate fields while for low pinning strengths the incommensurate field shows a nonlinear (sub-linear) increase due to vortex-vortex interactions which crosses over to a linear increase.

We find that at  $B/B_\phi = 1, 1/2$ , and  $1/4$ , where the vortex lattice is ordered, the depinning process and subsequent flow is elastic with the moving vortex lattice having the same symmetry as the pinned lattice. For fields near strong commensurability, and for  $B/B_\phi > 1$ , we observe a two-stage depinning process where vacancies or interstitial defects in the commensurate vortex crystal depin first, as can be seen in velocity versus driving force curves that are equivalent to experimental  $V(I)$  curves.

At the incommensurate fields, for  $B/B_\phi > 0.35$ , the vortex lattice depins plastically with only a portion of the vortices moving and the vortex motion occurring in winding paths in both the  $x$  and  $y$  directions. For these fields (vortex densities) at strong drives we observe *re-ordering* to an elastic distorted triangular moving lattice where the vortices move in *1D channels* along the pinning rows. For  $B/B_\phi < 0.35$  the initial depinning is still plastic but is followed by a transition to a channel flow phase where the vortices move in 1D channels along the pinning rows. In contrast to what occurs at higher fields, the individual 1D channels at lower fields contain different numbers of vortices, and the moving vortex lattice retains considerable positional disorder. These reordered phases are only stable in the strongly driven limit and we do not observe any hysteresis in the  $V(I)$  curves or vortex lattice order for either field range.

For triangular pinning arrays we find a different set of matching filling fractions than those found for square pinning. The effective pinning of the lattice is enhanced and an ordered vortex lattice appears at  $B/B_\phi = 1, 6/7, 2/3, 1/3, 1/4, 1/6$ , and  $1/7$ . Further, there is no peak in the critical depinning force at  $1/2$ . For strong pinning the vortex lattice at  $B/B_\phi = 1/2$  is disordered and all the vortices are located at pinning sites, while for weak disorder the vortex lattice at  $1/2$  has a square ordering in which half of the vortices are located at the inter-

stitial regions. For weak pinning the commensurability peaks in the critical depinning force are enhanced and an additional peak at  $B/B_\phi = 1/2$  is observed. For both strong and weak pinning the moving vortex lattice at  $B/B_\phi = 1/2$  is square. For the triangular pinning array we do not find any matching effects for  $B/B_\phi > 1$  which is due to the fact that the interactions with interstitial vortices cause a certain portion of the pinning sites to be left unoccupied. We observe  $V(I)$  characteristics and moving phases similar to the ones found in the square pinning array.

## II. SIMULATION

We model logarithmically interacting pancake vortices in a 2D superconductor interacting with square and triangular pinning arrays. The overdamped equation of motion for a vortex  $i$  is

$$\mathbf{f}_i = \frac{d\mathbf{r}_i}{dt} = \mathbf{f}_i^{vv} + \mathbf{f}_i^{vp} + \mathbf{f}_d = \mathbf{v}_i. \quad (1)$$

The vortex-vortex interaction potential is  $U_v = -\ln(r)$ . The total force on vortex  $i$  from the other vortices is  $f_i^{vv} = -\sum_{j \neq i}^{N_v} \nabla_i U_v(r_{ij})$ . We impose periodic boundary conditions and evaluate the periodic long-range logarithmic interaction with an exact sum [35]. Pinning is modeled as attractive parabolic wells of radius  $r_p$ ,

$$f_i^{vp} = -\sum_{k=1}^{N_p} (f_p/r_p)(\mathbf{r}_i - \mathbf{r}_k^{(p)}) \Theta((r_p - |\mathbf{r}_i - \mathbf{r}_k^{(p)}|)/\lambda) \quad (2)$$

Here, we measure distance in units of the penetration depth  $\lambda$ ,  $\mathbf{r}_k^{(p)}$  is the location of pinning site  $k$ ,  $f_p$  is the maximum pinning force, and  $\Theta$  is the Heaviside step function. The pinning is placed in a square or triangular array. The initial vortex positions are obtained by annealing from a high temperature configuration, with the vortices in a molten state, and slowly cooling to  $T = 0$ . This is intended to mimic field cooled experiments performed in [12,13]. We reduce the initial temperature to zero in twenty steps and remain at each step for  $1.5 \times 10^5$  MD steps, each being  $dt = 0.01$  in normalized units. The vortex configurations are insensitive to the waiting time for waiting times greater than  $5 \times 10^4$ . We note that the true ground states may only be attainable for prohibitively long waiting times; however, the agreement between our results and experiments is encouraging.

After the vortex configurations are obtained, the critical depinning force is determined by applying a slowly increasing, spatially uniform driving force,  $f_d$ , which would correspond to a Lorentz force from an applied current. For each drive increment we measure the average vortex velocity in the direction of drive,  $V_x = \sum_i^{N_v} \hat{\mathbf{x}} \cdot \mathbf{v}_i$ . The

force,  $f_d$ , versus velocity,  $V_x$ , curve corresponds experimentally to a voltage-current,  $V(I)$ , curve. The depinning force is defined to be the force value at which  $V_x$  reaches a value of 0.03 times the ohmic (linear) response.

## III. FRACTIONAL MATCHING FOR SQUARE PINNING ARRAY

In Fig. 1(a,b) we show the critical depinning force,  $f_p^c$ , versus the vortex density for a system with a pinning density of  $n_p = 1.36/\lambda^2$ ,  $f_p = 0.9f_0$ , and  $r_p = 0.3\lambda$ . In Fig. 1(a) we show  $f_p^c$  for magnetic fields up to  $B/B_\phi = 2.25$ , illustrating the matching effects at  $B/B_\phi = 1$  and 2 as well as clear matching effects at  $1/2$  and  $1/4$ . Figure 1(b) displays  $f_p^c$  for  $B/B_\phi < 0.6$ , where additional sub-matching peaks are visible at  $1/3$ ,  $1/6$ ,  $1/5$ , and  $1/8$ , with the  $1/3$  matching field being the largest of these. We do not observe any particular matching at  $2/3$  or  $4/5$ . Figure 2(a) shows the vortex positions (black circles) and pinning sites (open circles) for  $B/B_\phi = 1$ , where the vortices form a square lattice with the pinning sites. In Fig. 2(b), we show the vortex configuration at an incommensurate field,  $B/B_\phi = 0.64$ , where a peak in the critical depinning force is absent. Here, no apparent ordering in the vortex lattice can be observed. We also find that the vortex lattice is in general disordered at the other incommensurate fields. In Fig. 2(c), for  $B/B_\phi = 1/2$ , the vortices form an ordered checkerboard state of a single domain. This state was also observed in imaging experiments on vortices in superconductors [10,12,13] as well as of vortices in wire networks [36,37]. In the experiments by Field *et al.* [12], domains of two different orientations of the checkerboard state are found at  $B/B_\phi = 1/2$  where the domains of a single orientation are very large. It is unclear whether these domain structures in experiments result from some disorder at the pinning sites or are an intrinsic part of the vortex configurations as suggested by simulations of Josephson-junction arrays [38]. We have conducted larger simulations on systems with up to 392 vortices at  $B/B_\phi = 1/2$ ; however, we have found only single domains of vortices. In Fig. 2(d) the  $B/B_\phi = 1/3$  state is shown. Here the vortex configuration is not completely ordered; however, the vortices are generally positioned in diagonal stripes running along  $\pm 45^\circ$  separated by two empty diagonal stripes. This state looks almost identical to the results found in experiments [12,13]. Completely ordered states at the  $1/3$  filling have been predicted for repulsive particles on a square lattice as well as vortices in square networks [22,39]. The disorder in our system may come from having too short of an annealing time. We have tested annealing times from  $2.5 \times 10^5$  to  $5 \times 10^6$  normalized time units for  $B/B_\phi = 1/3$  and have not found any appreciable differences in the vortex configurations; neither have we found noticeable system size effects. We find that for weaker pinning, the diagonal

ordering becomes less prominent as some vortices begin to sit in the interstitial regions suggesting that, for our simulations and possibly for the experiments, the vortex-vortex interaction, which tends to make the vortex lattice triangular, causes the disorder. In subsection B we show more explicitly the role of the pinning strength on the vortex lattice ordering at the  $1/3$  matching field.

In Fig. 2(e) at  $B/B_\phi = 1/4$  the vortices form an ordered lattice with vortices occupying every other pinning site in every other row. In Fig. 2(f) we show the vortex lattice ordering at  $1/5$  which shows only regions of the square lattice ordering such as observed in the upper right area of Fig. 2(e). A similar ordering was observed in [12].

### A. $V(I)$ Characteristics

We show, in Fig. 3(a), a series of  $V(I)$  curves for  $B/B_\phi = 0.98, 1, 1.05,$  and  $1.2$ . The  $V(I)$  curve shows a single jump at the matching field. This is due to all the vortices depinning simultaneously. For  $B/B_\phi = 0.98$  we observe a two-stage depinning process with initial depinning due to the onset of vacancy motion in the  $B/B_\phi = 1$  commensurate vortex lattice, followed by depinning of the vortices at the pinning sites which is associated with the second jump in the vortex velocities. At  $B/B_\phi = 1.05$  the  $V(I)$  curves look similar to those obtained in previous simulations for vortices in bulk superconductors [40]. Here the pinned phase is considerably reduced compared to the  $1/1$  filling, and a two stage depinning process can be seen. The initial response is due to depinning of the interstitial vortices, and the second larger jump occurs when all the vortices begin to move. The additional jumps in the vortex velocities are due to transitions between different plastic flow phases which are discussed in more detail in Ref. [40]. For  $B/B_\phi = 1.2$  the two stage depinning features are still present and in general, for all  $B/B_\phi > 1$ , we observe the two depinning thresholds.

In Fig. 3(b) we show velocity versus driving force for  $B/B_\phi = 0.525, 0.5,$  and  $0.485$ . At  $1/2$  there is a single jump in  $V_x$  while at  $0.525$  and  $0.485$  the depinning transition occurs in two steps as seen in the initial jump in the  $V(I)$  followed by another larger jump. We find that two stage depinning occurs just above or below the matching fields where two distinct species of vortices exist: the vortices forming the commensurate structure at the matching fields, and the vacancies or interstitial vortices in the commensurate vortex structure. These vacancies and interstitials will have well defined depinning thresholds lower than those of the vortices forming the commensurate structure. For increasing or decreasing vortex density, relative to the  $1/2$  matching field, the overall vortex structure can change and the distinction between the two species of vortices is lost. In this case the two stage depinning transition disappears as seen in

the  $V(I)$  curves in Fig. 3(c) for  $B/B_\phi = 0.3$  and  $0.41$ . Here the two-stage depinning process is clearly absent.

### B. Dependence of Vortex Configurations on Pinning Strength

We have carried out a series of simulations at  $B/B_\phi = 1, 1/2, 1/3,$  and  $0.43$  with  $f_p$  ranging from  $0.1f_0$  to  $2.0f_0$ . The vortex configurations at  $B/B_\phi = 1$  and  $1/2$ , as seen in Fig. 1(a,b), are stable for all values of  $f_p$  we have examined. In principle, even at these fillings, for small pinning strength, the elastic interactions of the vortex lattice will dominate, and consequently the lattice will be triangular.

For  $B = 1/3$  and for  $f_p > 0.6f_0$  the vortex configuration is the partially disordered phase with alternating diagonal rows filled as seen in Fig. 2(d). For weaker  $f_p$  a portion of the vortices become located in the interstitial regions between the pinning sites. In Fig. 4(a) we show the vortices and the pinning sites and in Fig. 4(b) we show the vortices only for  $f_p < 0.5f_0$  where we observe an ordering when the vortex-vortex interaction is strong enough to induce triangular ordering; however, the vortex lattice can still take advantage of the periodicity of the pinning sites by allowing every other vortex to be pinned. In the ordered vortex lattice of Fig. 4(a), vortices fill every third pinning site in every other pinning row, while in the adjacent rows the vortices are not located in the pinning sites but instead are positioned in every third interstitial location. This produces a more triangular ordering in the vortex lattice which is easier to see in Fig. 4(b). As the pinning strength,  $f_p$ , is reduced for  $B/B_\phi = 0.43$ , we observe some vortices sitting at interstitial positions; however, we only observe regions of triangular ordering for the weakest pinning strength.

In Fig. 5 we plot the critical depinning force,  $f_p^c$ , versus pinning strength,  $f_p$ , for  $B/B_\phi = 1/2$  and  $0.43$ . Here,  $f_p^c$  increases linearly with  $f_p$  for the entire range of values considered, indicating that the vortices are in the single vortex pinning regime. Since the pinned vortex lattice is symmetric, this can be understood by realizing that the vortex-vortex interactions cancel and the depinning threshold will therefore be the pinning force strength,  $f_p$ . For  $B/B_\phi = 0.43$  the critical depinning force increases in a non linear fashion for low  $f_p$  and then becomes linear for high  $f_p$ . At  $B/B_\phi = 0.43$  the vortex lattice is disordered and the vortex-vortex interactions do not cancel, resulting in  $f_p^c$  always being less than  $f_p$ . The critical depinning force for  $B/B_\phi = 0.43$  is always less than that of  $1/2$  filling with the maximum difference occurring near  $f_p = 0.3$ .

#### IV. MOVING VORTEX STATES FOR SQUARE PINNING ARRAY

Figure 6 shows the vortex positions, pinning sites, and trajectories for the strongly driven vortex lattice for  $B/B_\phi = 1$  [Fig. 6(a,b)] and  $1/2$  [Fig. 6(c,d)]. Here we show that the moving vortex structures are the same as the pinned vortex structures seen in Fig. 2. The depinning at  $1/1$ ,  $1/2$ , and  $1/4$  filling fractions occurs elastically with vortices retaining the same neighbors they had at depinning. The vortices are also seen to flow in 1D channels along the pinning sites.

For incommensurate fields,  $B/B_\phi > 0.35$ , the initial depinning is plastic with vortices wandering in both the  $x$  and  $y$  directions. A transition to an ordered moving vortex lattice is found at higher drives. In Fig. 7 we show the vortex flow patterns for increasing driving force at  $B/B_\phi = 0.64$ . Just above depinning at  $f_d = 0.805$  [Fig. 7(a)], the vortex flow is plastic with the vortices wandering in both the  $x$  and  $y$  directions. For stronger drives,  $f_d/f_0 = 0.85$  [Fig. 7(b)], the vortices begin to flow in 1D channels along the pinning sites; however, there is still considerable hopping from one channel to the next. For  $f_d/f_0 = 0.9$  [Fig. 7(c)], the vortex lattice is almost completely reordered with only occasional vortex jumps between adjacent channels. For  $f_d = 1.0$  [Fig. 7(d)], the vortex lattice is completely reordered and the vortices flow in strict 1D channels along the pinning sites. In Fig. 8 we show the vortex positions for  $f_d/f_0 = 0.805$  [Fig. 8(a)], where the vortex lattice is clearly disordered, and  $f_d/f_0 = 1.0$  [Fig. 8(b)], where the vortex lattice has a defect-free distorted square ordering. The reordered vortex lattice can be frozen into the zero drive state by abruptly shutting off the driving; however, if the drive is slowly decreased the vortex lattice will re-enter the plastic flow phase and disorder so no hysteresis is observed in the  $V(I)$  curves.

For  $B/B_\phi < 0.35$  we find that the moving vortex lattice does not completely reorder. In Fig. 9(a) we show the vortex positions, pinning sites, and trajectories for  $B/B_\phi = 0.28$  which indicate that the vortices are flowing elastically in 1D channels along the pinning rows, but the number of vortices can differ from channel to channel. In Fig. 9(b) the moving vortex lattice can be seen to retain a considerable amount of disorder. We have found that for weaker pinning the field at which the vortices can completely reorder is reduced below  $B/B_\phi = 0.35$ .

#### V. FRACTIONAL VORTEX MATCHING AND DYNAMICS FOR TRIANGULAR PINNING ARRAYS

In Fig. 10 we show the critical depinning force versus field for a system with triangular pinning. Matching effects can be seen at  $B/B_\phi = 1, 6/7, 2/3, 1/3, 1/4$ , and

$1/7$ . No depinning peak is seen for the  $1/2$  matching nor for  $B/B_\phi > 1$ . In Fig. 11(a) we show the matching fields at  $B/B_\phi = 1$ , where all the vortices are pinned forming a triangular lattice. In Fig. 11(b), for  $B/B_\phi = 2/3$ , we find a honeycomb vortex lattice with vacancies forming a triangular lattice, which is the same as the vortex lattice configuration at the  $1/3$  matching field [Fig. 11(d)]. In Fig. 11(c), at  $B/B_\phi = 1/2$ , no particular vortex lattice ordering is observable. In Fig. 11(e), for  $B/B_\phi = 1/3$ , the vortices form a triangular sublattice. In Fig. 11(f), at  $B/B_\phi = 1/4$ , the vortices again form a triangular lattice while in Fig. 11(e), at  $B/B_\phi = 1/7$ , the overall vortex lattice is mostly triangular with some defects. The vortex lattice configuration at  $B/B_\phi = 1/7$  (not shown) has a triangular configuration with a vacancy lattice the same as the vortex lattice in Fig. 11(e).

#### A. Vortex Pinning and Ordering for Weaker Pinning Strength

As was shown in Fig. 11(c), the vortex configuration at  $B/B_\phi = 1/2$  is disordered. In Fig. 12(a) we show that, for a weaker pinning strength of  $f_p/f_0 = 0.3$ , an ordered state, in which half of the vortices are located in the interstitial regions between the pinning sites and the other half are located at the pinning sites, is possible for  $B/B_\phi = 1/2$ . This gives the overall vortex lattice a square symmetry which is evident in Fig. 12(b).

In Fig. 13 we show  $f_p^c$  versus vortex density for  $f_p/f_0 = 0.3$  for a more limited field range of  $0 < B/B_\phi < 0.6$ . Here  $f_p^c$  is considerably reduced from that of  $f_p/f_0 = 0.9$ ; however, the commensurability peaks are stronger with a larger difference between the commensurate peaks and the incommensurate regions. In addition to finding the same commensurability peaks observed at  $B/B_\phi = 1/3, 1/4$ , and  $1/7$ , we now clearly observe peaks at  $1/6, 1/9$ , and  $1/2$ . Most experiments in periodic pinning arrays have found that commensurability effects are strongest very near  $T_c$  where the pinning is the weakest. For decreasing temperature, the overall pinning increases, but the clear matching anomalies gradually vanish. One possibility (in the experiments) is that the bulk pinning becomes relevant for lower  $T$ ; however, experiments without dots or holes, for the same temperature regions, find that the critical current is much *lower* than in the system with the pinning arrays, indicating the strong pinning is coming from the dots or holes. Our simulations suggest that the increasing pinning force of the dots alone can wash out the matching anomalies even in the absence of bulk pinning. Figure 8 shows that the relative difference between the  $f_p^c$  for a commensurate and incommensurate fields is maximum for low  $f_p$  and is constant for higher  $f_p$ . The relative height of the commensurate peak can be

expressed as

$$\delta f_p^c = \frac{(f_p^c(\text{com}) - f_p^c(\text{incom}))}{f_p^c(\text{incom})} = \frac{d_c^p}{f_p^c(\text{incom})}.$$

For large  $f_p$ ,  $d_c^p$  will be constant and  $f_p^c(\text{incom}) \propto f_p$  so  $\delta f_p^c$  will decrease as  $\sim 1/f_p$ .

The peak at  $1/2$  occurs due to the formation of the ordered vortex lattice as seen in Fig. 12. An experimental test for the presence of this phase would be the appearance of an anomaly at  $B/B_\phi = 1/2$  in a triangular pinning array as  $T$  approaches  $T_c$ .

### B. Vortex Ordering for $1 < B/B_\phi < 1.5$

In Fig. 14 we show the vortex configuration and pinning sites at  $B/B_\phi = 4/3$ , where it might be expected that the interstitial vortex lattice will resemble the vortex configuration at the  $B/B_\phi = 1/3$  matching field. Fig. 14 shows that a number of pinning sites are actually unoccupied with two vortices sitting adjacent to the pinning sites and caged in by six adjacent vortices. This indicates that placing an interstitial vortex between two vortices at the pinning sites is costly enough to depin one of the vortices. These types of defects disrupt any kind of overall interstitial vortex lattice ordering so that higher field fractional matching effects cannot be observed. For stronger pinning sites all the pinning sites will be occupied so fractional matching may be possible.

The general  $V(I)$  characteristics are similar to those found in the square pinning arrays with a two step depinning process for  $B/B_\phi > 1$  and within 0.05 flux-density of the sub-matching fields. We also find that the general features of the vortex dynamics and reordering are similar to those found with the square pinning array.

## VI. CONCLUSION

We have investigated fractional matching effects in thin-film superconductors with square and triangular arrays of pinning sites. For the square arrays we find matching effects in the form of enhanced critical depinning forces at  $B/B_\phi = 1, 3/4, 1/2, 1/3, 1/4,$  and  $1/5$ . The observed vortex configurations at these fields are in good agreement with recent imaging experiments. The vortex configurations also depend on the strength of the pinning sites. The vortex configuration at the  $1/3$  matching field can have a transition from a diagonally ordered lattice to a distorted triangular lattice, where every other vortex is interstitially pinned rather than being located in a pinning site.

We also find that the critical depinning current scales linearly with  $f_p$ . Since the vortex lattice at the commensurate fields is symmetric, the vortex-vortex interactions

cancel and the vortex lattice is always in the individual vortex pinning regime. For large  $f_p$ , the critical depinning force for the incommensurate fields also scales linearly with deviations from linearity at low  $f_p$  as vortex-vortex interactions become relevant.

Near  $B/B_\phi = 1, 1/2,$  and  $1/4$  the  $V(I)$  characteristics show a two-stage depinning which is due to the presence of two well defined vortex species: the vortices of the commensurate lattice configurations, and the interstitials or vacancies in that lattice, which have different depinning thresholds. For  $B/B_\phi > 1$ , a two stage depinning in the  $V(I)$  curves is always observed.

We find that the vortex lattice depins elastically at commensurate fields where the vortex lattice is symmetric; e.g., at  $B/B_\phi = 1, 1/2,$  and  $1/4$ , while at the incommensurate fields the vortex lattice first undergoes plastic flow where the vortices flow in a random manner, and then at a higher drive reorders and flows elastically in well defined 1D channels along the pinning sites. For  $B/B_\phi < 0.35$ , vortices will still flow elastically along the pinning sites; however, there is considerable disorder in the vortex lattice. For weaker pinning the vortex lattice will reorder for fields  $B/B_\phi < 0.35$ .

We have also investigated triangular pinning arrays and find matching effects at  $B/B_\phi = 1, 6/7, 2/3, 1/3, 1/4, 1/5,$  and  $1/7$ , which show ordered vortex lattices, while  $1/2$  and other incommensurate fillings show disordered vortex lattices. For  $B/B_\phi < 0.5$  and for weaker pinning, we observe additional matching at  $2/7$  and  $1/6$  as well as a general enhancement of the other commensurate peaks. For the weaker pinning we also find a commensuration peak at  $B/B_\phi = 1/2$ , which occurs due to the formation of an ordering state where half the vortices are located in the interstitial regions so the overall vortex arrangement is square. The presence of these ordered states should be observable in magnetization curves.

For triangular pinning arrays, with  $B/B_\phi > 1$ , we do not observe any matching features due to certain pinning sites remaining vacant where a pair of vortices can rotate around the vacant pinning site. We observe similar  $V(I)$  characteristics and dynamics for the triangular pinning array as seen in the square arrays.

The static states for the pinning arrays should be observable with Hall-probe arrays, Bitter decoration and Lorentz microscopy. Similar techniques may also be able to observe the dynamics; particularly at strong drives when the vortices should move in well defined 1D channels along the pinning. The motion of interstitials or vacancies near commensurate fields can be tested experimentally by looking for multiple depinning stages in the current-voltage curves.

### Acknowledgements

We thank C.J. Olson for critical reading of this manuscript and S. Bending, S. Field, F. Nori, C.J. Ol-

son, I.K. Schuller, and G.T. Zimányi for useful discussions. This work was supported by NSF-DMR-9985978, by the Director, Office of Advanced Scientific Computing Research, Division of Mathematical, Information and Computational Sciences of the U.S. Department of Energy under contract number DE-AC03-76SF00098 as well as by CLC and CULAR (Los Alamos National Laboratory/ University of California).

- 
- [1] G. Blatter *et al.*, *Rev. Mod. Phys.* **66**, 1125 (1994).  
 [2] A.T. Fiory, A.F. Hebard, and S. Somekh, *Appl. Phys. Lett.* **32**, 73 (1978).  
 [3] M. Baert *et al.*, *Phys. Rev. Lett.* **74**, 3269 (1995); V.V. Moshchalkov *et al.*, *Phys. Rev. B* **54**, 7385 (1996); V.V. Moshchalkov *et al.*, *Phys. Rev. B* **57**, 3615 (1998); V.V. Metlushko *et al.*, *Europhys. Lett.* **41**, 333 (1998); V.V. Metlushko *et al.*, *Phys. Rev. B* **59**, 603 (1999); L. Van Look *et al.*, *Phys. Rev. B* **60**, R6998 (1999).  
 [4] V.V. Metlushko *et al.*, *Solid State Commun.* **91**, 331 (1994).  
 [5] M. Baert *et al.*, *Europhys. Lett.* **29**, 157 (1995).  
 [6] V.V. Metlushko *et al.*, *Phys. Rev. B* **60**, R12585 (1999).  
 [7] T. Puig *et al.*, *Phys. Rev. B* **58**, 5744 (1998).  
 [8] E. Rosseel *et al.*, *Phys. Rev. B* **53**, R2983 (1996).  
 [9] J.Y. Lin *et al.*, *Phys. Rev. B* **54**, R12714 (1996); A. Castellanos *et al.*, *Appl. Phys. Lett.* **71**, 962 (1997); R. Surdeanu, R.J. Wijngaarden, R. Wordenweber, and R. Griessen, *to be published*.  
 [10] K. Harada *et al.*, *Science* **271**, 1393 (1996).  
 [11] V.V. Metlushko *et al.*, *Phys. Rev. B* **60**, R12 585 (1999).  
 [12] S. Field *et al.*, *cond-mat/0003415*.  
 [13] S. Bending *et al.*, *to be published*.  
 [14] J.I. Martín *et al.*, *Phys. Rev. Lett.* **79**, 1929 (1997); Y. Jaccard *et al.*, *Phys. Rev. B* **58**, 8232 (1998).  
 [15] A. Hoffman, P. Prieto and I.K. Schuller, *Phys. Rev. B* **61**, 6958 (2000).  
 [16] D.J. Morgan and J.B. Ketterson, *Phys. Rev. Lett.* **79**, 1929 (1998).  
 [17] Y. Fasano *et al.*, *Phys. Rev. B* **60**, R15047 (1999).  
 [18] A. Terentiev, D.B. Watkins, L.E. De Long, D.J. Morgan and J.B. Ketterson, *Physica C* **324**, 1 (1999); A. Terentiev *et al.*, *Phys. Rev. B* **61**, R9249 (2000).  
 [19] J.I. Martín *et al.*, *Phys. Rev. Lett.* **83**, 1022 (1999).  
 [20] L.D. Cooley and A.M. Grishin, *Phys. Rev. Lett.* **74**, 2788 (1995).  
 [21] C. Reichhardt, C.J. Olson, and F. Nori, *Phys. Rev. B* **57**, 7937 (1998).  
 [22] S. Teitel and C. Jayaprakash, *Phys. Rev. Lett.* **51**, 1999 (1993).  
 [23] G.I. Watson, *Physica A* **246**, 253 (1997).  
 [24] A.E. Koshelev and V.M. Vinokur, *Phys. Rev. Lett.* **73**, 3580 (1994).  
 [25] T. Giamarchi and P. Le Doussal, *Phys. Rev. Lett.* **76**, 3580 (1996); **78**, 752 (1997); P. Le Doussal and T. Giamarchi, *Phys. Rev. B* **57**, 11 356 (1998).  
 [26] L. Balents, M.C. Marchetti, and L. Radzihovsky, *Phys. Rev. Lett.* **78**, 751 (1997); *Phys. Rev. B* **57**, 7705 (1998); S. Scheidl and V.M. Vinokur, *Phys. Rev. E* **57**, 2574 (1998).  
 [27] H.J. Jensen, A. Brass and A.J. Berlinsky, *Phys. Rev. Lett.* **60**, 1676 (1988); A.-Shi and A.J. Berlinsky, *Phys. Rev. Lett.* **67**, 1926 (1991); N. Grønbech-Jensen, A.R. Bishop, and D. Domínguez, *Phys. Rev. Lett.* **76**, 2985 (1996); S. Ryu *et al.*, *Phys. Rev. Lett.* **77**, 5114 (1996); M.C. Faleski, M.C. Marchetti, and A.A. Middleton, *Phys. Rev. B* **54**, 12477 (1996); S. Spencer and H.J. Jensen, *Phys. Rev. B* **55**, 8473 (1997); C.J. Olson, C. Reichhardt and F. Nori, *Phys. Rev. Lett.* **81**, 3757 (1998); D. Domínguez, *Phys. Rev. Lett.* **82**, 181 (1999).  
 [28] K. Moon, R.T. Scalettar and G.T. Zimányi, *Phys. Rev. Lett.* **77**, 2278 (1996); C.J. Olson and C. Reichhardt, *Phys. Rev. B* **61**, 3811 (2000).  
 [29] M.J. Higgins and S. Bhattacharya, *Physica C* **257**, 232 (1996); M.C. Hellerqvist *et al.*, *Phys. Rev. Lett.* **76**, 4022 (1996); W. Henderson *et al.*, *Phys. Rev. Lett.* **77**, 2077 (1996).  
 [30] F. Pardo *et al.*, *Science* **396**, 349 (1998).  
 [31] A.M. Troyanovski, J. Aarts, and P.H. Kes, *Nature* **399**, 665 (1999).  
 [32] C. Reichhardt and F. Nori, *Phys. Rev. Lett.* **82**, 414 (1999).  
 [33] V.I. Marconi and D. Domínguez, *Phys. Rev. Lett.* **82**, 4922 (1999); V.I. Marconi *et al.*, *cond-mat/0001392*.  
 [34] K.D. Fisher, D. Stroud and L. Janin, *Phys. Rev. B* **60**, 15371 (1999).  
 [35] N. Grønbech-Jensen, *Comp. Phys. Comm.* **119**, 115 (1999).  
 [36] K. Runge and B. Pannetier, *Europhys. Lett.* **24**, 737 (1993).  
 [37] H.D. Hallen *et al.*, *Phys. Rev. Lett.* **71**, 3007 (1993).  
 [38] N. Grønbech-Jensen, F. Falo, A. R. Bishop, and P. S. Lomdahl, *Phys. Rev. B* **45**, 10139 (1992).  
 [39] F. Falo, A. R. Bishop, and P. S. Lomdahl, *Phys. Rev. B* **41**, 10983 (1990).  
 [40] C. Reichhardt, C.J. Olson and F. Nori, *Phys. Rev. B* **58**, 6534 (1998).

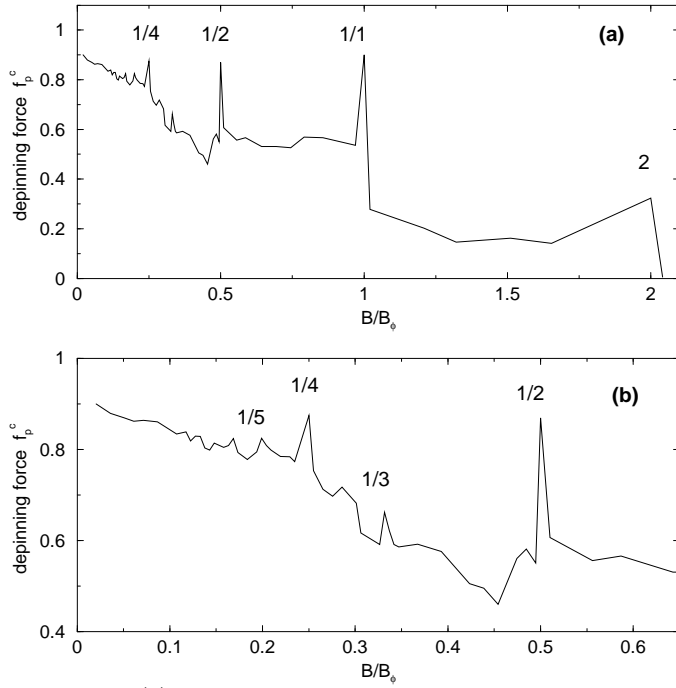


FIG. 1. (a) Critical depinning force  $f_p^c$  versus vortex density  $B/B_\phi$  for  $0 < B/B_\phi < 2.1$  with a square pinning array. Peaks can be seen in  $f_p^c$  at  $B/B_\phi = 1/4, 1/2, 1/1$ , and  $2/1$ . (b) Critical depinning force for the system in (a) for  $0 < B/B_\phi < 0.6$  showing narrowed view of the peaks in  $f_p^c$  for  $B/B_\phi = 1/5, 1/4, 1/3$ , and  $1/2$ . Smaller peaks can also be seen at  $B/B_\phi = 2/7, 1/6$ , and  $1/8$ .

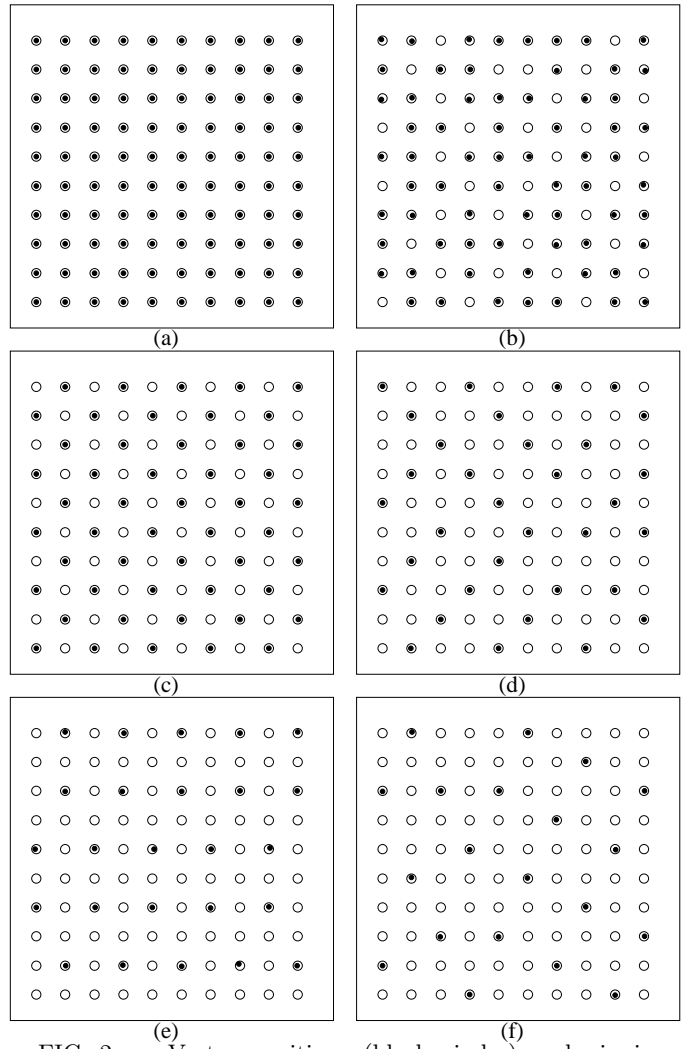


FIG. 2. Vortex positions (black circles) and pinning sites (open circles) from the simulation in Fig. 1 for (a)  $B/B_\phi = 1/1$ , (b), 0.642, (c)  $1/2$ , (d)  $1/3$ , (e)  $1/4$ , and (f)  $1/5$ .

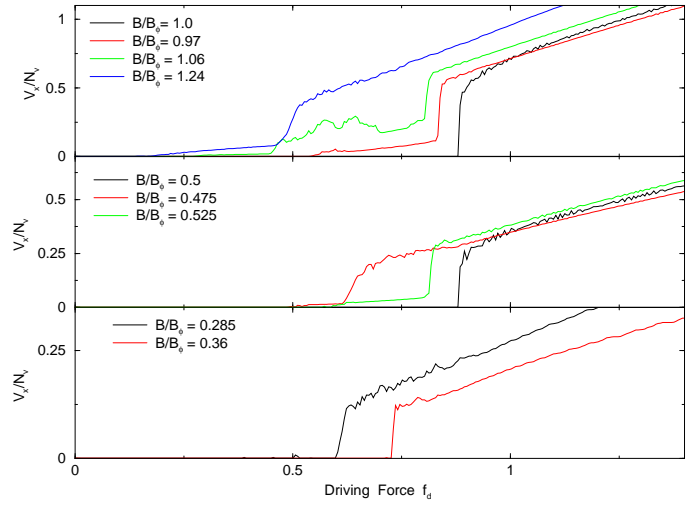


FIG. 3. Vortex velocities  $V_x$  versus the applied driving force  $f_d$  for (a)  $B/B_\phi = 0.98, 1.0, 1.06$ , and  $1.23$ . The largest critical depinning force occurs for the  $1/1$  matching. (b)  $B/B_\phi = 0.525, 0.5$ , and  $0.485$ . (c)  $B/B_\phi = 0.30$  and  $0.41$ .

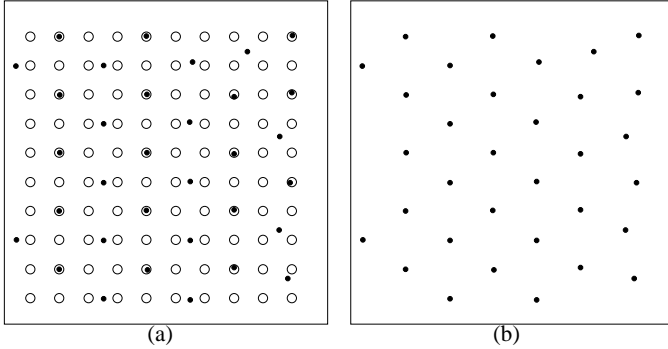


FIG. 4. (a) Vortex positions and pinning sites. (b) Vortex positions only for  $B/B_\phi = 1/3$  with  $f_p/f_0 = 0.3$ . Unlike the case for  $f_p/f_0 = 0.9$  (Fig. 2(e)), where all the vortices are located at pinning sites, roughly half the vortices are located at the interstitial regions between the pinning sites so that the overall vortex structure is a distorted square as seen in (b).

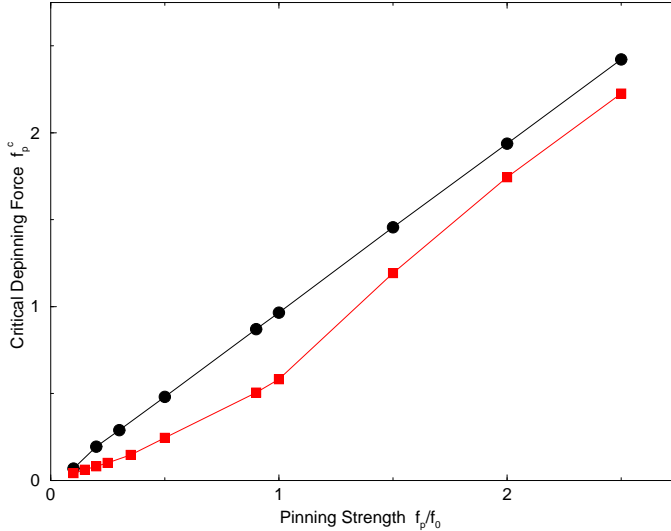


FIG. 5. Critical depinning force versus  $f_p$  for  $B/B_\phi = 1/2$  (upper curve) and  $B/B_\phi = 0.642$  (lower curve). For  $1/2$  filling  $f_p^c$  goes linearly with  $f_p$  for the entire range of  $f_p$  investigated. For  $0.642$  filling  $f_p^c$  is linear in  $f_p$  for large values of  $f_p$  but is non-linear for low  $f_p$ . A maximum difference between the two curves occurs near  $f_p/f_0 = 0.4$ .

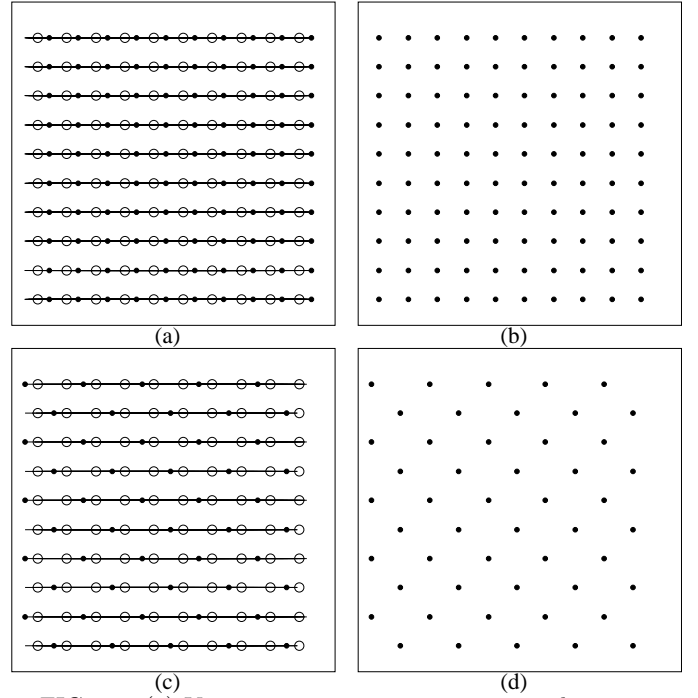


FIG. 6. (a) Vortex positions, pinning sites, and trajectories for the moving vortex lattice at  $B/B_\phi = 1$ . (b) Vortex positions showing the moving square vortex lattice. (c) Vortex positions, pinning sites and trajectories for the moving system at  $B/B_\phi = 1/2$ . (d) Vortex positions showing the square moving vortex lattice rotated at  $45^\circ$  with respect to the pinning lattice. In both cases the moving lattice has the same symmetry as the pinned lattice. Further, the vortex motion can be seen to flow in well defined 1D channels along the pinning sites.

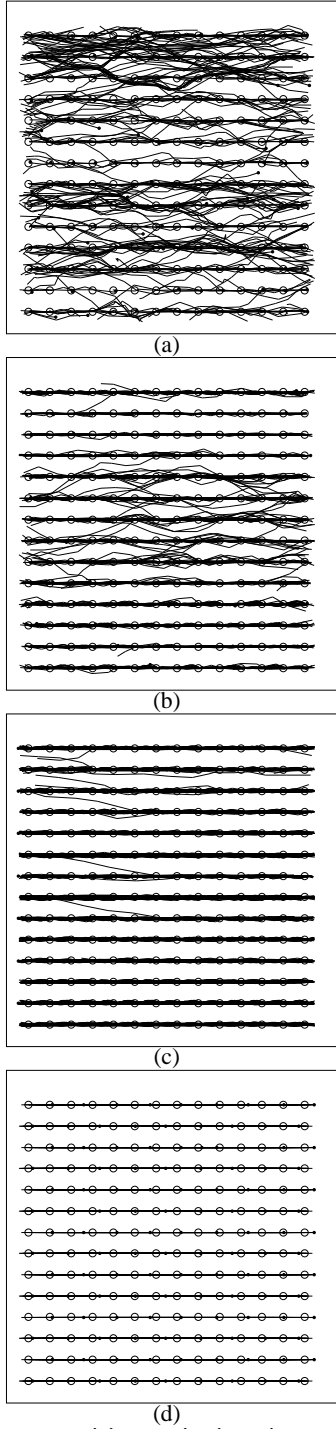


FIG. 7. Vortex positions, pinning sites, and trajectories for  $B/B_\phi = 0.6428$  for increasing applied driving force  $f_d$ . (a) For  $f_d/f_0 = 0.8$ , just above depinning, plastic flow occurs with vortices flowing in both  $x$  and  $y$  directions. (b) At  $f_d/f_0 = 0.9$  the vortex motion is increasingly along the pinning sites forming 1D channels. (c) At  $f_d/f_0 = 0.95$ , almost all vortex flow is along the pinning sites with only occasional jumping of vortices between channels. (d) At  $f_d/f_0 = 1$ , the vortex lattice has completely reordered. Vortices flow plastically with the flow restricted to 1D channels along the pinning sites.

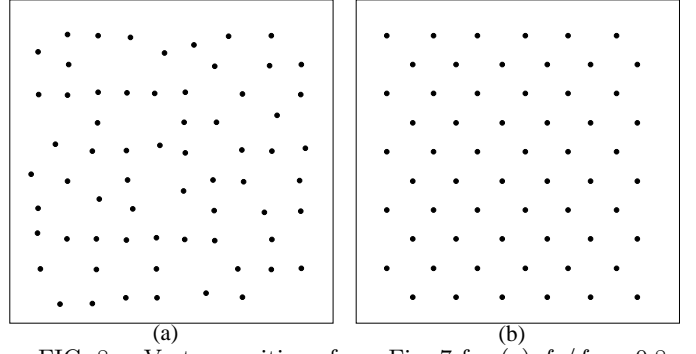


FIG. 8. Vortex positions from Fig. 7 for (a)  $f_d/f_0 = 0.8$  and (b)  $f_d/f_0 = 1.0$ . The strongly driven vortex lattice reorders to a distorted square lattice.

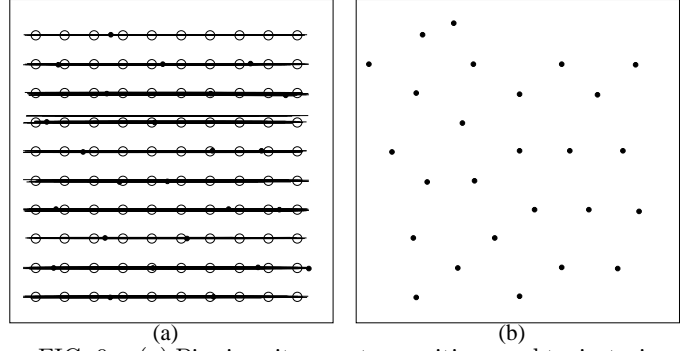


FIG. 9. (a) Pinning sites, vortex positions and trajectories for  $B/B_\phi = 0.28$  for  $f_d/f_0 = 1$ . The vortices flow elastically in 1D channels; however, the number of vortices is not equal in each channel. (b) Snapshot of the vortex positions, showing that the moving vortex lattice retains a considerable amount of disorder.

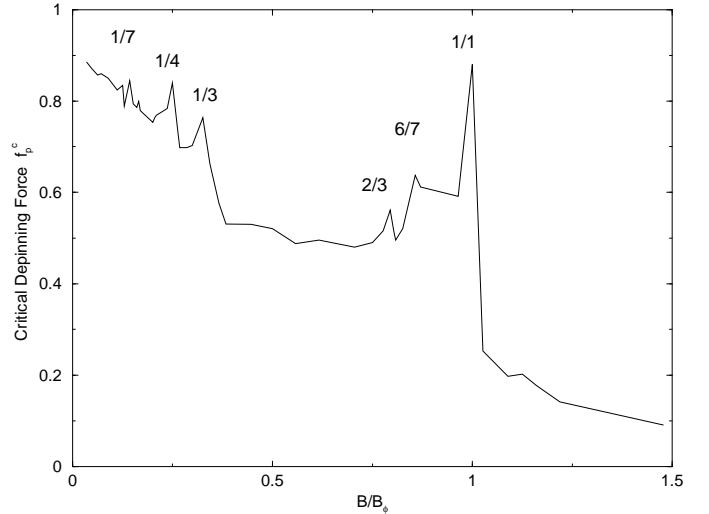


FIG. 10. Critical depinning force  $f_p^c$  versus vortex density for a triangular pinning array. Commensuration peaks can be seen at  $B/B_\phi = 1/1, 6/7, 2/3, 1/3, 1/4,$  and  $2/7$ . Note that there is no peak at  $B/B_\phi = 1/2$ .

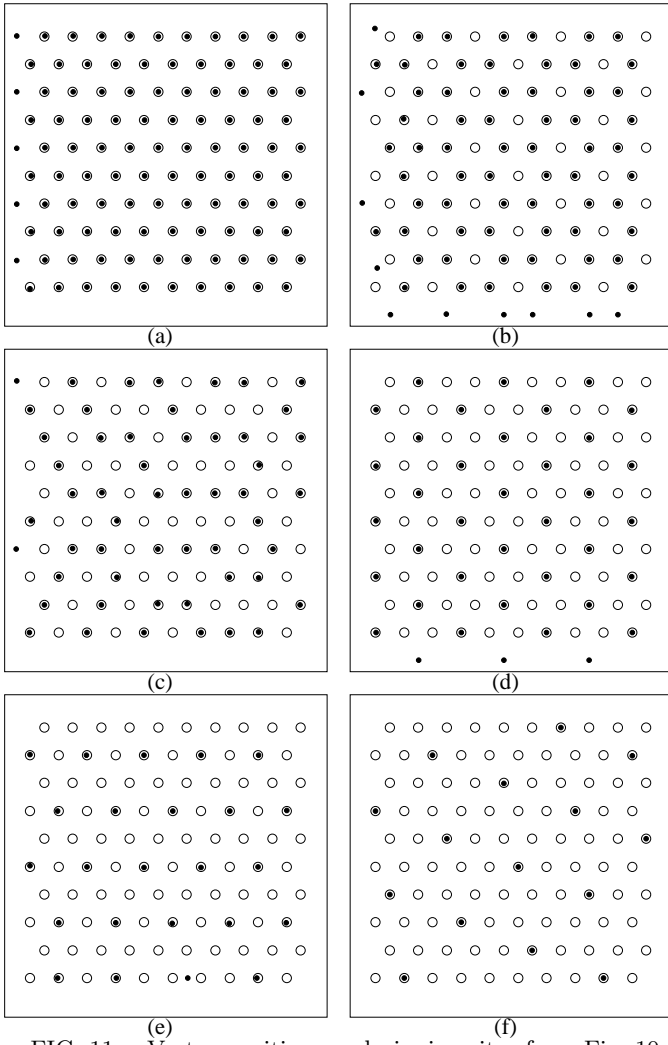


FIG. 11. Vortex positions and pinning sites from Fig. 10 for (a)  $B/B_\phi = 1/1$ , (b)  $2/3$ , (c)  $1/2$ , (d)  $1/3$ , (e)  $1/4$ , and (f)  $1/7$ .

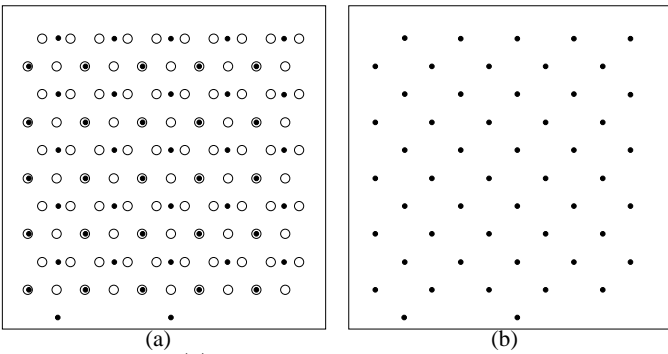


FIG. 12. (a) Vortex positions and pinning sites at  $B/B_\phi = 1/2$  and (b) vortex positions only for  $f_p/f_0 = 0.3$ . In (a), only half of the vortices are located at pinning sites with the other half located at the interstitial regions. In (b) the overall vortex lattice has a square symmetry.

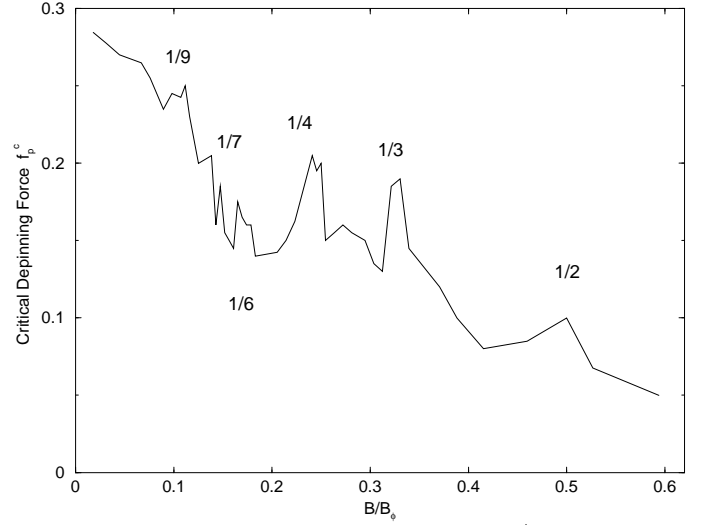


FIG. 13. Critical depinning force for  $f_p^c/f_0 = 0.3$  for  $0 < B/B_\phi < 0.6$ . Commensurate peaks are observed at  $B/B_\phi = 1/4, 1/3, 1/6, 2/7, 1/7$ , and  $1/9$ . A peak at  $B/B_\phi = 1/2$  is now visible with the vortices forming the ordered state observed in Fig. 10.

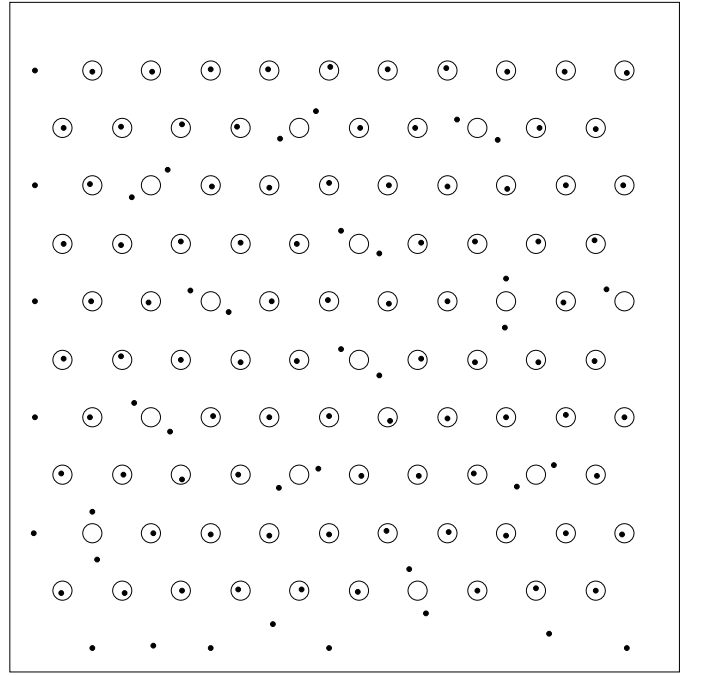


FIG. 14. Vortex positions and pinning sites at  $B/B_\phi = 1.25$  showing that several of the pinning sites are unoccupied.